In situ thermal conductivity of gas-hydrate-bearing sediments of the Mallik 5L-38 well

J. Henninges and E. Huenges
Section Geothermics, GeoForschungsZentrum Potsdam, Potsdam, Germany

H. Burkhardt
Fachgebiet Angewandte Geophysik, Technische Universität Berlin, Berlin, Germany

Received 17 March 2005; revised 22 July 2005; accepted 7 September 2005; published 29 November 2005.

[1] Detailed knowledge about thermal properties of rocks containing gas hydrate is required in order to quantify processes involving gas hydrate formation and decomposition in nature. In the framework of the Mallik 2002 program, three wells penetrating a continental gas hydrate occurrence under permafrost were successfully equipped with permanent fiber-optic distributed temperature sensing cables. Temperature data were collected over a 21-month period after completing the wells. Thermal conductivity profiles were calculated from the geothermal data as well as from a petrophysical model derived from the available logging data and application of mixing law models. Results indicate that thermal conductivity variations are mainly lithologically controlled with a minor influence from hydrate saturation. Average thermal conductivity values of the hydrate-bearing sediments range between 2.35 and 2.77 W m^{-1} K^{-1}. Maximum gas hydrate saturations can reach up to about 90% at an average porosity of 0.3.

Citation: Henninges, J., E. Huenges, and H. Burkhardt (2005), In situ thermal conductivity of gas-hydrate-bearing sediments of the Mallik 5L-38 well, *J. Geophys. Res.*, *110*, B11206, doi:10.1029/2005JB003734.

1. Introduction

[2] The thermal properties of hydrate-bearing rocks are a controlling factor for all processes involving the formation and decomposition of gas hydrate in nature, which are inevitably coupled with the transport of heat within the formation. The thermal conductivity of pure hydrate is about 20% lower than the thermal conductivity of water and up to 80% lower than that of ice. Because of the low thermal conductivity of pure hydrate it has often been proposed that the presence of gas hydrate should have a significant influence on the bulk rock thermal conductivity and the geothermal gradient within hydrate-bearing formations [e.g., *Ruppel*, 2000]. Until now, however, there is a lack of thermal conductivity data measured on rock samples and only a limited number of laboratory measurements on artificially produced samples have been published.

[3] The direct measurement of thermal conductivity on hydrate-bearing rock samples is generally hampered by the difficulties and uncertainties arising from possible degradation of hydrate during sample retrieval and preparation. Laboratory experiments have to be designed to simulate in situ conditions in order to maintain the proportion of the phases present within the sample.

[4] *Stoll and Bryan* [1979] performed measurements of the thermal conductivity of mixtures of sand, water, gas, and hydrate. They concluded that the thermal conductivity of a propane hydrate saturated sand with 40% porosity was reduced about 23% compared to water saturated conditions. *Waite et al.* [2002] performed measurements of thermal conductivity on porous mixtures of methane hydrate and quartz sand with varying percentages of hydrate content. They concluded that the bulk rock thermal conductivity was influenced by two different effects: Increases of the bulk rock thermal conductivity were interpreted as the result of enhanced intergranular contact, while decreases were attributed to the low thermal conductivity of the hydrate itself.

[5] Here we investigate the influence of methane hydrate on the transport of heat in porous rocks, on the basis of analysis of geophysical borehole logging data collected during the Mallik 2002 Gas Hydrate Production Research Well Program [*Dallimore et al.*, 2002; *Dallimore and Collett*, 2005; *Henninges et al.*, 2005]. The in situ thermal conductivity is estimated using two independent approaches: First, the effective thermal conductivity of hydrate-bearing sediments is calculated using different mixing law models in combination with methods of formation evaluation from well log data. Second, thermal conductivity profiles are calculated from the measured geothermal gradients and an estimate of local heat flow on the basis of Fourier's law of heat conduction.

2. Geology, Permafrost, and Gas Hydrate Occurrences

[6] Within the framework of the Mallik 2002 Program, three wells named JAPEX/JNOC/GSC et al. Mallik 3L-38, 4L-38, and 5L-38, spaced at 40 m, were drilled to a depth of about 1200 m. The Mallik 2002 program was preceded by

0148-0227/05/2005JB003734$09.00

Table 1. Depths to Top of Lithological Units of Cored Interval of Mallik 5L-38[a]

		Core Depth, m	Log Depth, m		
Unit	Description	5L-38	3L-38	5L-38	4L-38
I	sand with silt and pebble interbeds	885.6	885.6	885.6	885.6
II	silt and low-rank coal	932.6	931.0	930.5	932.2
III	sand with silt and pebble interbeds	944.4	942.6	942.4	944.3
IV	silt and low-rank coal	1004.7	1001.6	1002.3	1002.5
V	sand	1087.6	1085.0	1085.2	1087.5
VI	silt with sand and clay interbeds	1142.7	1135.8	1141.3	1135.2

[a]Lithological units and core depths after *Medioli et al.* [2005]. The correlation of coring and logging data was performed on the basis of the available gamma ray logs.

the drilling of the Mallik 2L-38 well in 1998 [*Dallimore et al.*, 1999], as well as the hydrocarbon exploratory well Mallik L-38 in 1972 [*Bily and Dick*, 1974].

[7] The Mallik site is located in the Mackenzie-Delta area in the northwestern part of arctic Canada, close to the coast of the Beaufort Sea. The gas hydrate accumulations occur within a sedimentary succession between about 800 m and 1100 m below ground level, which is overlain by a thick permafrost layer extending to a depth of about 600 m below ground level.

[8] A series of high- and low-amplitude seismic reflectors was interpreted as an interbedded succession of hydrate-bearing sandstones and nonhydrate-bearing shale layers [*Collett et al.*, 1999]. The hydrate-bearing strata at Mallik have been assigned to the Mackenzie Bay and Kugmallit sequences of Oligocene and early Miocene age [*Dallimore and Collett*, 1999]. The lithology of the core samples retrieved from the Mallik 2L-38 and 5L-38 wells generally varied between unconsolidated sands and gravels, to compact sandstones and shales. *Medioli et al.* [2005] identified six informal lithological units within the cored interval of the Mallik 5L-38 well between 885.63 and 1150.79 m (Table 1). The depths of the coring data were correlated to the well logs using the available gamma ray logs. The lithological units can laterally be traced between the three Mallik 2002 wells with only minor offsets in depth. Within the succession of sand- and silt-dominated sedimentary units a number of thin (0.1 m to 1.7 m) dolomite cemented sandstones and low-rank coal beds occur.

[9] It should be noted that depth specifications in this study are given relative to the rotary kelly bushing, which is 4.6 m above ground level, or 5.6 m above sea level, unless otherwise indicated.

3. Distributed Temperature Measurements

[10] Within recent years, fiber-optic distributed temperature sensing (DTS) has been introduced as a new technology for measuring borehole temperatures [e.g., *Hurtig et al.*, 1993; *Förster et al.*, 1997]. Through the deployment of DTS technology, quasi-continuous temperature profiles can be measured with high temporal resolution. Short laser pulses are injected into an optical fiber and the temperature distribution is calculated from the backscattered and reflected light signal [*Hartog and Gamble*, 1991].

3.1. Installation of Sensor Cables and Logging Schedule

[11] The three Mallik 2002 wells were equipped with permanent fiber-optic sensor cables [*Henninges et al.*, 2005]. In the two lateral observation wells, the sensor cables were installed to a depth of 1158 m in order to determine the formation temperatures. In the central Mallik 5L-38 well, temperatures were measured to about 940 m depth and online temperature monitoring during a thermal stimulation experiment was performed [*Hancock et al.*, 2005].

[12] A special feature of the experimental design at Mallik is the permanent installation of the sensor cables behind the borehole casing. After completion of the well, the sensor cables are located in the cement annulus between casing and borehole wall (Figure 1).

[13] The DTS logging was started one to two days after completion of the respective well and continuous monitoring of the well temperatures was performed over a period of up to 61 days between January and March 2002, using the DTS 800 M10^{TM} manufactured by Sensa, U.K. Two subsequent DTS surveys were carried out for long-term temperature monitoring in October 2002 and September 2003 with a temporary setup of the DTS equipment. In total, the borehole temperatures were recorded over a period of 21 months after drilling of the wells.

[14] Further details about the installation procedure and the temperature logging program are given by *Henninges et al.* [2005].

3.2. Processing of Temperature Data

[15] In order to generate temperature profiles which can be compared to the other available borehole data, the raw DTS temperature data were correlated to the elevation of the rotary kelly bushing (KB) on the drill floor as a common depth datum. The depth values were calculated with reference to the known positions of the casing connectors, the depths of which were picked from the casing-collar-locator logs (CCL). In the Mallik 5L-38 well, the distinct temperature signal of the perforating gun was used for the depth correlation because the position of the end of the sensor cable was not exactly known due to a fiber break [see *Hancock et al.*, 2005].

[16] Under controlled conditions within the laboratory, the measured temperatures showed an accuracy of ±0.3 K after calibration. The accuracy of the measured temperature data was verified by independent downhole temperature measurements with an electronic memory tool deployed in the 3L-38 and 4L-38 wells.

[17] The temperature resolution is proportional to the square root of integration time. After completing the measurements, the temperature data were averaged over approximately 2 hour intervals resulting in a temperature resolution of about 0.06 K.

[18] The stacked temperature data were filtered using the fast Fourier transformation (FFT) eliminating coherent

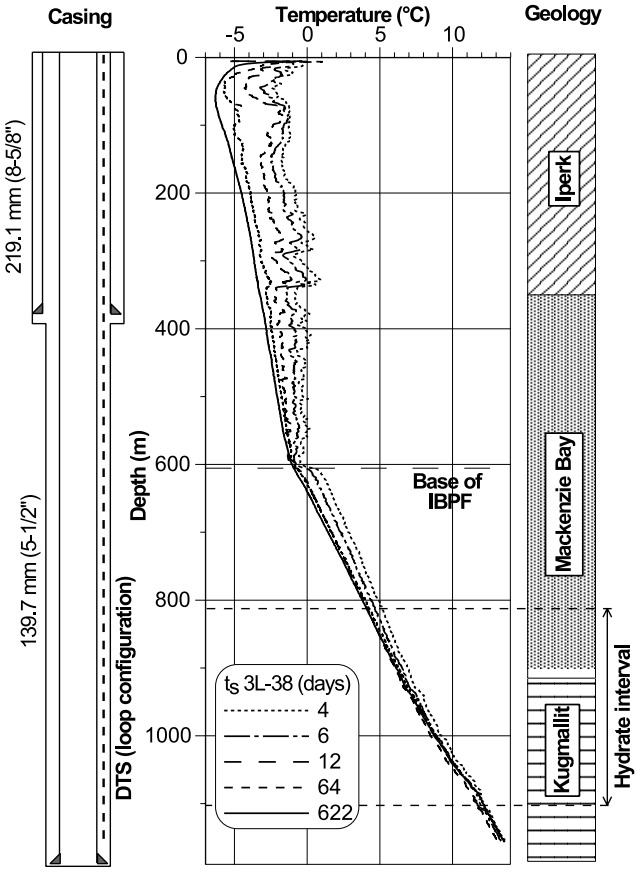

Figure 1. Schematic well profile of the Mallik 3L-38 observation well, temperature profiles for successive times after completion of the well (t_s), and sequence boundaries [from *Dallimore et al.*, 1999]. IBPF, base of ice-bearing permafrost; DTS, distributed temperature sensing.

noise generated by the DTS instrument. In order to reduce the random noise prior to evaluation, the resulting FFT-filtered temperature profile data were additionally smoothed using a three-point running average filter (Figure 2). The estimated temperature resolution of the processed DTS data is 1.70×10^{-2} K for Mallik 3L-38 and 2.60×10^{-2} K for Mallik 4L-38 and 5L-38. The different noise levels associated with the temperature data are mainly attributed to the different DTS measurement modes used for the specific wells, which are referred to as single-ended and double-ended measurement processing modes.

[19] Temperature gradient profiles were constructed from the slopes of linear fits for the September 2003 temperature profiles over 5-m intervals. The standard error (standard deviation) σ_Γ of the 5-m temperature gradients is 2.6 K km^{-1} for the Mallik 3L-38 well, and 4.0 K km^{-1} for the Mallik 4L-38 and 5L-38 wells.

3.3. Measurement Results

[20] Excerpts from the recorded temperature data are displayed in Figure 1 as temperature profiles for successive points in time after the cementing of the Mallik 3L-38 well (shut-in time t_s). As a result of the thermal disturbance due to the drilling process, the borehole temperature gradually equilibrated to the temperature of the surrounding formation during the 21-month logging period. The analysis of the temperature data from the 3L-38 and 4L-38 wells using the Horner plot method showed that the well temperatures measured during the September 2003 DTS survey have returned to about ±0.1 K from equilibrium with the formation temperatures [*Henninges et al.*, 2005]. The measured changes of temperature with depth from the September 2003 DTS survey are therefore approximately equal to the geothermal gradient.

[21] The September 2003 temperature profiles of the three wells all show very similar characteristics. The temperature field in the deeper subsurface is characterized by a pronounced increase of the geothermal gradient below the base of the ice-bearing permafrost (Figure 1), which was determined to lie at a depth between 604 ± 3.5 m and 609 ± 3.5 m [*Henninges et al.*, 2005]. The following discussion focuses on the interval of the hydrate-bearing strata, which occur below the base of the permafrost within a depth between about 900 m and 1100 m.

[22] Depth profiles of the temperature gradients calculated from the measured borehole temperature data within the zone of the gas hydrate occurrences are displayed in Figure 3. Below the base of the ice-bearing permafrost, the mean temperature gradient within the Mackenzie Bay Sequence is about 23.5–24.1 K km^{-1}. Below about 920 m, the geothermal gradient shows distinct variations and locally increases over 40 K km^{-1}. The onset of this interval containing zones of increased geothermal gradients appears in all three wells and correlates with the boundary between the Mackenzie Bay and Kugmallit sequences, which lies at the transition between unit I and unit II at a depth of about 930 m (Table 1). Individual sections of the geothermal gradient profiles exhibit a good correlation between the wells. As commonly observed, the geothermal gradient correlates with the gamma ray log. Sand-dominated units, marked by low gamma ray intensities, characteristically have a higher thermal conductivity than silt- or clay-dominated units with high gamma ray intensities.

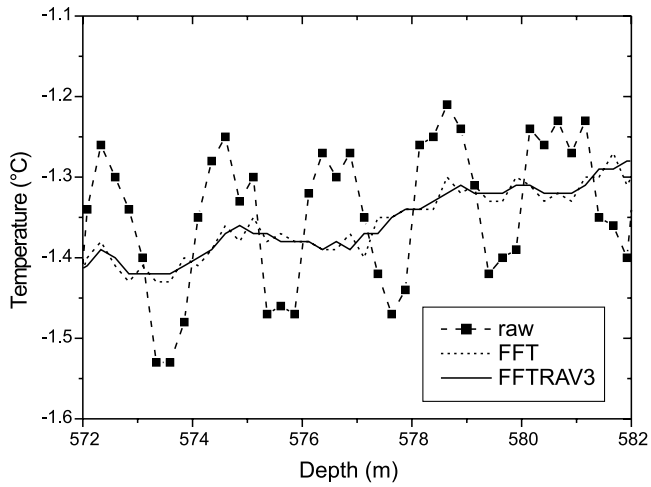

Figure 2. Comparison of raw and filtered DTS temperature data. Raw indicates DTS temperature profile, 2 hour integration time; FFT indicates FFT-filtered temperature profile; FFTRAV3 indicates FFT-filtered temperature profile smoothed with three-point running average filter.

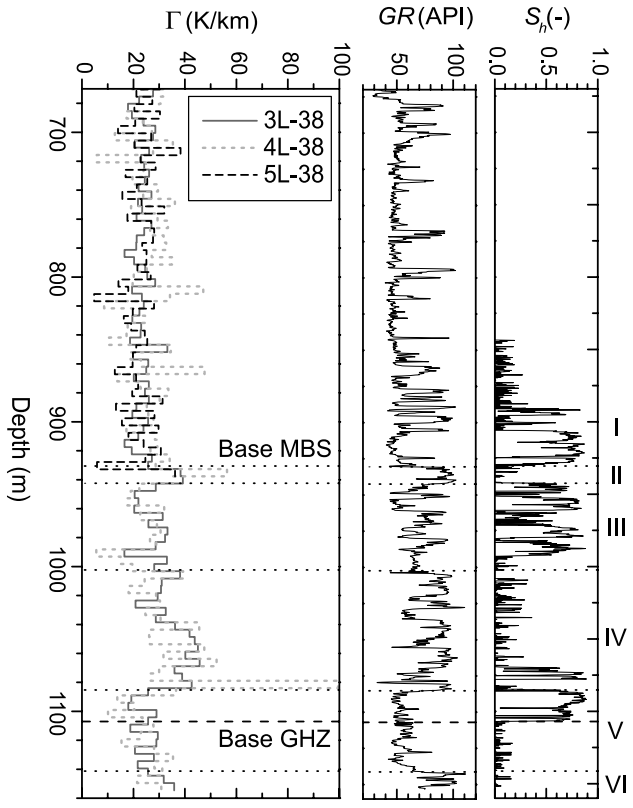

Figure 3. Detail of 5-m average temperature gradients (Γ) within the zone of the gas hydrate occurrences (GHZ). GR is gamma ray intensity, Mallik 5L-38; S_h is gas hydrate saturation (fraction of total porosity) estimated from difference of density-porosity and NMR-porosity logs of Mallik 5L-38 well (DMR method, see text for further details). Roman numerals indicate lithological units adopted from *Medioli et al.* [2005]. The transition between unit I and unit II marks the boundary between the Mackenzie Bay Sequence (MBS) and the underlying Kugmallit Sequence.

The six lithological units exhibit characteristic changes of the temperature gradient profiles, reflecting their respective lithological composition (Figure 3): The silt-dominated units (II, IV, and VI) are characterized by higher geothermal gradients relative to the sand-dominated units (I, III, and V). Intermittent sand and silt layers can also be traced within the geothermal gradient profiles. In contrast to this, there is no apparent correlation of the temperature gradient and the estimated hydrate saturation.

4. A Petrophysical Rock Model From Logging Data

[23] In a simplified model, hydrate-bearing sediments occurring in permafrost environments below the permafrost base can be thought of as being composed of four main components [*Collett*, 2001]: The sediment matrix is composed of sand and shale, and the pore space is filled by water and/or gas hydrate (Figure 4). According to the petrophysical measurements performed on core samples from Mallik, there is strong evidence that gas hydrate is forming a discontinuous phase within the pore fluid [*Kulenkampff and Spangenberg*, 2005].

[24] The volumetric proportions of each of the components are subject to changes resulting from variations in lithology and hydrate saturation. The volumetric composition, i.e., mineral content of the sediment matrix, porosity, and saturation of the pore filling phases, were estimated from the available geophysical logging data.

4.1. Shale Content

[25] Clay minerals, feldspar, and organic matter within the silt grain fraction can act as a source of radioactivity because of their content of naturally occurring isotopes of ^{40}K, ^{232}Th, and ^{238}U. The shale content of a succession of sedimentary rocks is therefore often determined from the gamma ray log reading. The local gamma ray intensity GR is linearly scaled between the minimum and maximum gamma ray intensities, which are equal to the gamma ray readings in a pure sand and a pure shale within the rock type under investigation:

$$\mathrm{GRI} = \frac{\mathrm{GR} - \mathrm{GR_{min}}}{\mathrm{GR_{max}} - \mathrm{GR_{min}}} \tag{1}$$

Depending on sediment type, age, and degree of consolidation, the shale content V_{sh} is then calculated as a function of the gamma ray index GRI. For the Mallik sediments, the following relation was used, which was derived empirically for weakly consolidated sediments of tertiary and younger age [e.g., *Rider*, 1996]:

$$V_{sh} = 0.083\left(2^{3.7\mathrm{GRI}} - 1\right) \tag{2}$$

The uranium, thorium, and potassium concentrations from the Schlumberger Hostile Natural Gamma Ray Sonde™ logs (HNGS) were analyzed for indications on the source of the natural gamma radiation. For the most part, the gamma ray curve compensated for uranium content (HCGR) runs parallel to the standard gamma ray curve (HSGR, Figure 5). Therefore there is no indication of zones with anomalously high uranium concentrations, e.g., resulting from enrichment of U-bearing heavy minerals, and the HSGR log was used for the calculation of V_{sh}.

[26] The calculated V_{sh} values were calibrated using the available grain size analysis data from 213 core samples from the Mallik 5L-38 well [*Medioli et al.*, 2005]. The

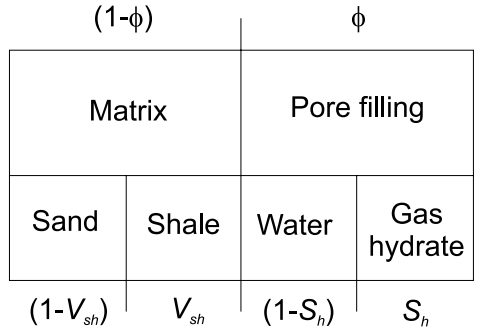

Figure 4. Model for hydrate-bearing sediment in a permafrost environment below the permafrost base, modified after *Collett* [2001]. The ϕ is porosity; V_{sh} is shale content; and S_h is hydrate saturation.

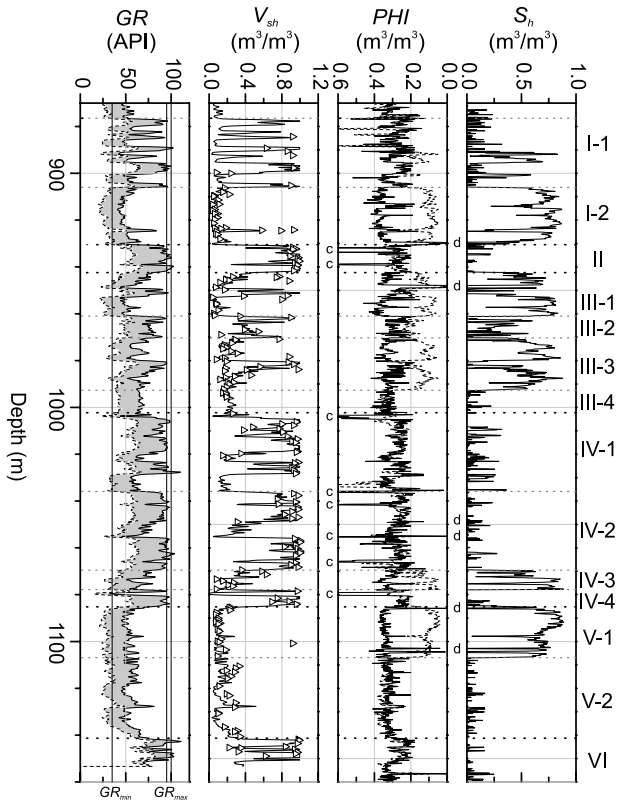

Figure 5. Montage of Mallik 5L-38 well logs for estimation of shale content, porosity, and gas hydrate saturation. GR is gamma ray logs (solid line, standard gamma ray, HSGR; dashed line, computed gamma ray corrected for uranium content, HCGR). V_{sh} is shale volume, calculated from HCGR log using equation for tertiary unconfined rocks; rectangles are silt fraction (<0.063 mm) from grain size analyses of Mallik 5L-38 core samples (data from *Medioli et al.* [2005]). PHI is apparent porosity (solid line, gamma-gamma density log apparent porosity, DPHI; dashed line, magnetic resonance apparent porosity, TCMR). S_h is density magnetic resonance method gas hydrate saturation. The c is coal, and d is dolomite-cemented sandstone. Roman numerals indicate lithological units adopted from *Medioli et al.* [2005].

GR_{min} and GR_{max} values in equation (1) were manually adjusted until a good fit with the measured silt grain fractions was achieved (Figure 5).

4.2. Porosity and Gas Hydrate Saturation

[27] *Kleinberg et al.* [2003] have proposed the density-magnetic resonance (DMR) method to determine the gas hydrate saturation from geophysical well logs. The DMR method was also applied using the well logs of the Mallik 5L-38 well [*Kleinberg et al.*, 2005]. The hydrate saturations estimated using the DMR method show a good agreement with the results of measurements on core samples, where the hydrate saturation was determined from the weight loss during decomposition [*Kulenkampff and Spangenberg*, 2005].

[28] Nuclear magnetic resonance (NMR) logging tools respond quantitatively to pore space liquid water but not to gas hydrate [*Kleinberg et al.*, 2003]. With the DMR method, the gas hydrate saturation S_h is computed from the difference between gamma-gamma density log apparent porosity, *DPHI*, and the magnetic resonance apparent porosity, *TCMR* [*Kleinberg et al.*, 2005]:

$$S_h = \frac{\mathrm{DPHI} - \mathrm{TCMR}}{\mathrm{DPHI} + \alpha \mathrm{TCMR}} \tag{3}$$

where

$$\alpha = \frac{\rho_w - \rho_h}{\rho_{ma} - \rho_w} \tag{4}$$

and ρ_w, ρ_h, and ρ_{ma} are the densities of water, hydrate, and the sediment matrix, respectively.

[29] The effect of the density contrast between gas hydrate and water on the density porosity can be taken into account with the following equation for the true porosity ϕ:

$$\phi = \frac{\mathrm{DPHI} + \alpha \mathrm{TCMR}}{1 + \alpha} \tag{5}$$

However, because of the relatively small density contrast between gas hydrate and water, strong effects will only occur at high porosities (i.e., >40%) and high gas hydrate saturations (i.e., >50%).

[30] Exceptions to the application of the DMR method described above are individual intervals containing layers of low-rank coal and dolomite-cemented sandstones. These intervals can clearly be recognized on the available geophysical well logs, a part of which is displayed in Figure 5. The low-rank coal beds are characterized by low gamma ray intensities, low densities, high neutron porosities and high resistivities. The dolomite-cemented sandstone beds were identified by high densities, high resistivities, low neutron and NMR porosities. Because of the strong density contrast compared to other rock-forming materials, the DMR method is not applicable here and the computed gas hydrate saturation was set to zero within the affected intervals.

[31] The computed gas hydrate saturations are displayed in Figure 5. Ten individual hydrate-bearing zones with thicknesses between 1 m and 23 m, and average gas hydrate saturations between 25% and 68% were identified using the DMR method. Significant gas hydrate accumulations predominantly occur inside the sandstone units, with maximum saturations of up to 89%.

5. Estimation of the in Situ Thermal Conductivity

[32] Information about the in situ thermal conductivity of the formation can generally be derived by three different methods: (1) measurements on rock samples, (2) in situ temperature measurements, and (3) calculation from petrophysical models. In the framework of the Mallik 2002 program, only a very limited number of direct measurements of thermal conductivity on hydrate-bearing rock samples was carried out [*Wright et al.*, 2005]. Therefore, within this study the in situ thermal conductivity was estimated from petrophysical models as well as from the measured geothermal gradient.

[33] Petrophysical models can again be grouped into three different categories [e.g., *Somerton*, 1992]: The thermal

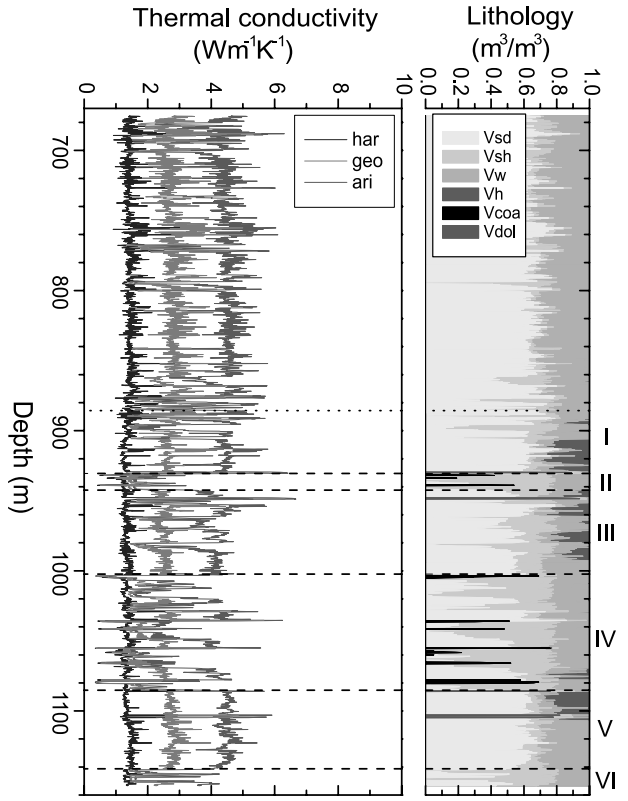

Figure 6. Comparison of thermal conductivity profiles for Mallik 5L-38 well calculated from arithmetic, geometric, and harmonic mean mixing law models. Lithological composition is derived from logging data. Roman numerals indicate lithological units adopted from *Medioli et al.* [2005]. See color version of this figure at back of this issue.

conductivity can be estimated from rock composition (mixing law models), geophysical logging data (empirical models), and theoretical models. Empirical or theoretical models for the thermal conductivity of hydrate bearing sediments have not been developed until now, therefore the in situ thermal conductivity was calculated using different mixing law models.

5.1. Thermal Conductivity Profiles From Mixing Law Models

[34] A significant amount of literature is devoted to the physical properties of frozen soils, which could represent an equivalent to hydrate-bearing sediments, apart from the contrast of thermal conductivity between ice and hydrate. A compilation of methods for calculating the thermal conductivity of soils with special consideration of freezing effects is given by *Farouki* [1981]. The method proposed by *Johansen* [1975] was found to be among the best methods for frozen saturated soils. For this soil type, the thermal conductivity is calculated from the volume fraction of ice, unfrozen water, quartz, and other minerals which summarize the remaining part of the sediment matrix using the geometric mean model described below.

5.1.1. Method

[35] Mixing law models are based on the concept that the effective properties of a multicomponent system can be calculated as the average value of the properties of the components and their volumetric fraction of the bulk rock composition. Different averaging methods can be applied depending on the arrangement of the components relative to each other [e.g., *Beck*, 1988].

[36] The weighted arithmetic mean model and the harmonic mean model are physically based models, which can be derived for heat flowing parallel and perpendicular to the structure in a layered medium. Within this study they were used to define the upper and lower limits of the physically possible scale of values.

[37] The effective properties of a random distribution of the components can be estimated using the geometric mean model, which was derived empirically for aggregates with low contrasts of thermal conductivity below a factor of 20 [*Woodside and Messmer*, 1961]. Within this study, the geometric mean model was chosen in order to test its applicability to hydrate-bearing sediments.

[38] The thermal conductivity was calculated using the following formulas for the arithmetic, harmonic, and geometric mean models [e.g., *Beck*, 1988]:

$$\lambda_{\mathrm{ari}} = \sum v_n \lambda_n \tag{6}$$

$$\lambda_{\mathrm{har}} = \frac{1}{\sum v_n / \lambda_n} \tag{7}$$

$$\lambda_{\mathrm{geo}} = \Pi \lambda_n^{v_n} \tag{8}$$

where λ_{ari}, λ_{har}, λ_{geo} are the effective thermal conductivities calculated from the respective mixing law model, and λ_n and v_n are the thermal conductivities and volume fractions of the respective components.

[39] The volumetric composition of the formation was determined from the available logging data using the different methods of formation evaluation described above. The individual volume fractions relative to the total rock volume were computed using the following set of equations (Figure 4):

$$v_{sd} = (1 - \phi)(1 - V_{sh}) \tag{9}$$

$$v_{sh} = (1 - \phi) V_{sh} \tag{10}$$

$$v_w = \phi (1 - S_h) \tag{11}$$

$$v_h = \phi S_h \tag{12}$$

The subscripts *sd*, *sh*, *w*, and *h* refer to sand, shale, water, and hydrate fraction, respectively.

[40] Although only of limited extent (Figures 5 and 6), special attention had to be devoted to the intervals containing low-rank coal and dolomite-cemented sandstone beds because of the strong density contrast compared to other rock-forming materials. Within the concerned intervals, the following procedure was applied: The true porosity ϕ was

Table 2. Thermal Conductivities of Components for Mixing Law Models

Component	Thermal Conductivity, W m^{-1} K^{-1}
Sand	7.0
Shale	1.9
Water	0.6
Hydrate	0.49
Coal	0.3
Dolomite	7.0

set equal to the magnetic resonance apparent porosity TCMR (see section 4.2). The shale volume v_{sh} was calculated as usual from equation (10), and the remaining volume of the rock matrix was assumed to be composed of coal or dolomite, respectively, resulting in a computation of v_{coal} and v_{dol} equal to v_{sd} from equation (9).

[41] Table 2 contains a list of the thermal conductivity values used for the calculation of the effective thermal conductivities. The thermal conductivity of the hydrate of ethylene oxide, like methane hydrate a structure I type, was determined as 0.49 ± 0.02 W m^{-1} K^{-1} at 263 K [*Cook and Laubitz*, 1981]. The influence of different guest molecules on the physical properties of a specific hydrate structure can as a first approximation be considered as small [*Sloan*, 1998]. Because the temperature at which the value of *Cook and Laubitz* [1981] was determined is rather close to the in situ temperature of the sediments under investigation of approximately 9°C (Figure 1), the thermal conductivity of methane hydrate was chosen as 0.49 W m^{-1} K^{-1} within this study.

[42] Except for water and methane hydrate, where the values of the pure substances were used, effective thermal conductivities of the mineral mixtures, which are represented by each component, were used. The effective thermal conductivity of shale was calculated from the average mineral composition determined by X-ray diffraction analysis (Table 3) and literature values of the thermal conductivities of the mineral components using the harmonic mean model. Here, the harmonic mean model was chosen because of the preferentially layered structure which can be assumed for the shale fraction resulting from the contained sheet silicates and the compaction of the sediments. The value for sand was chosen about 10% lower than the value of pure quartz, accounting for a small amount of impurities from other minerals like carbonates or feldspar, which is consistent with the procedures of other authors [e.g., *Revil*, 2000].

5.1.2. Results

[43] The thermal conductivity profiles calculated using the three different mixing law models are displayed in Figure 6. An attempt to quantify the uncertainty associated with the results of the mixing law models was not made because of the empirical nature of some of the underlying calculations (section 4) and the absence of appropriate comparative values. *Farouki* [1981] reported an accuracy of ±35% for the results produced by the method of *Johansen* [1975], which for saturated soils is equivalent to the geometric mean model applied in this work.

[44] The arithmetic mean model results in the highest and the harmonic mean model in the lowest values of thermal conductivity (Figure 6). Intermediate values of thermal conductivity were calculated from the geometric mean model. The largest differences of the results occur in the sand-dominated sections of the profile, whereas similar values were calculated for the sections containing a high amount of shale. This is consistent with the results of other authors: *Beck* [1988] states that at low contrasts of thermal conductivity (i.e., below a factor of 5) all three of the above models show similar results and the values calculated using the geometric mean model approximately fall into the middle of the scale of values.

[45] Table 4 contains a compilation of the average thermal conductivity values of the different lithological units, which were further subdivided according to the hydrate saturation of individual intervals (see Figure 5). The average thermal conductivity values calculated using the geometric mean model range between about 1.4–2.0 W m^{-1} K^{-1} within the shale-rich units ($V_{sh} > 0.5$) and about 2.2–2.8 W m^{-1} K^{-1} within the sand-dominated units ($V_{sh} < 0.5$). The lowest values were calculated for the sporadic coal-bearing sections, ranging between about 0.4–1.0 W m^{-1} K^{-1}. Maximum values between about 4.0–5.9 W m^{-1} K^{-1} were calculated for the isolated layers of dolomite-cemented sandstones.

5.2. Thermal Conductivity Profiles From Geothermal Data

5.2.1. Method

[46] Assuming constant heat flow by conduction, the bulk rock thermal conductivity in vertical direction λ_{zz} can be calculated from the measured geothermal gradient Γ and an estimate of the local heat flow q by a simple rearrangement of the one-dimensional form of Fourier's equation:

$$\lambda_{zz} = \frac{q}{\Gamma} \tag{13}$$

It should be pointed out that the success of this procedure is strongly dependent on the validity of the above stated assumption, as well as the quality of the heat flow estimate. The applicability of this method can only be proved by

Table 3. Average Mineral Composition[a]

Mineral	Minimum	Maximum	Average
Smectite and/or expandable MLC	0.03	0.21	0.10
Mica (Illite/Muscovite)	0.09	0.35	0.20
Kaolinite	0.06	0.23	0.16
Chlorite (Clinochlore)	0.06	0.20	0.15
Quartz	0.13	0.69	0.38
Feldspars (K-, Na-)	0.00	0.08	0.02

[a]Weight fraction, calculated from the results of 18 X-ray diffraction analyses of the clay grain fraction of shale samples from the Mallik 5L-38 well (data from *Medioli et al.* [2005]); MLC, mixed layer clays.

Table 4. Average Calculated Thermal Conductivity Values and Lithological Data of Subsections of Lithological Units Derived From Well Logs of the Mallik 5L-38 Well[a]

Unit	Top, m	Bottom, m	Thickness, m	V_{sh}	ϕ	S_h	λ_{ari}	λ_{geo}	λ_{harm}	λ_{zz} 3L-38	λ_{zz} 4L-38	λ_{zz} 5L-38
I-1	876.50	906.02	29.52	0.41	0.28	0.16	3.63	2.42	1.43	2.17 ± 0.32	2.16 ± 0.32	2.26 ± 0.33
I-2	906.02	930.50	24.48	0.10	0.33	0.66	4.54	2.79	1.41	2.66 ± 0.39	2.33 ± 0.34	2.88 ± 0.42
II	930.50	942.40	11.90	0.84	0.26	0.02	1.87	1.50	1.19	1.48 ± 0.22	1.32 ± 0.19	1.60 ± 0.25
III-1	942.40	961.03	18.63	0.24	0.30	0.52	4.20	2.71	1.53	2.30 ± 0.33	2.36 ± 0.34	n/a
III-2	961.03	970.33	9.30	0.50	0.27	0.21	3.37	2.21	1.39	1.95 ± 0.28	2.18 ± 0.32	n/a
III-3	970.33	992.73	22.40	0.33	0.31	0.52	3.83	2.38	1.32	2.00 ± 0.29	2.32 ± 0.34	n/a
III-4	992.73	1002.30	9.57	0.23	0.32	0.02	4.13	2.58	1.44	2.02 ± 0.29	2.57 ± 0.37	n/a
IV-1	1002.30	1035.90	33.60	0.56	0.28	0.04	2.96	2.05	1.35	1.86 ± 0.27	2.09 ± 0.30	n/a
IV-2	1035.90	1069.54	33.64	0.72	0.27	0.02	2.34	1.72	1.26	1.38 ± 0.20	1.54 ± 0.22	n/a
IV-3	1069.54	1077.77	8.23	0.27	0.30	0.57	4.06	2.50	1.35	1.70 ± 0.25	2.72 ± 0.40	n/a
IV-4	1077.77	1085.20	7.43	0.66	0.25	0.05	1.87	1.44	1.12	1.12 ± 0.16	1.03 ± 0.15	n/a
V-1	1085.20	1106.88	21.68	0.10	0.32	0.67	4.58	2.82	1.40	2.40 ± 0.35	2.68 ± 0.39	n/a
V-2	1106.88	1141.30	34.42	0.13	0.32	0.02	4.48	2.83	1.50	2.19 ± 0.32	2.42 ± 0.35	n/a
VI	1141.30	1153.36	12.06	0.69	0.26	0.01	2.69	1.94	1.37	1.96 ± 0.29	1.92 ± 0.28	n/a

[a]Values are in W m^{-1} K^{-1}.

evidence from independent data, which in the current study was supplied in the form of the petrophysical data derived from well log interpretation.

[47] The temperature profiles measured at Mallik in September 2003 have returned close to equilibrium with the formation temperature and the changes of temperature with depth are approximately equal to the geothermal gradient (section 3.3). For the calculation of the bulk rock thermal conductivities, the 5-m average temperature gradient profiles and a heat flow value of 55 ± 8 mW m^{-2}, which was derived by *Majorowicz and Smith* [1999] for the nearby Mallik L-38 well, were used. The standard errors σ_λ (standard deviation) of the resulting thermal conductivity values calculated from the relative errors of the temperature gradient σ_Γ (section 3.2) and heat flow σ_q are 18%, 23%, and 25% for the Mallik 3L-38, 4L-38, and 5L-38 wells, respectively.

5.2.2. Results

[48] The calculated 5-m thermal conductivity profiles are displayed in Figure 7, together with the 95% confidence limits, which are equal to $2\sigma_\lambda$. Table 4 contains a compilation of the average thermal conductivity values of the different lithological units which were further subdivided according to the hydrate saturation of individual intervals.

[49] The scatter of values is generally much greater for the Mallik 4L-38 and 5L-38 wells compared to the Mallik 3L-38 well. This is interpreted as a result of the different level of noise associated with the DTS temperature data (section 3.2). Above the base of the ice-bearing permafrost, the calculated conductivity values exhibit a much greater variability than within the underlying sequence of rocks. This is partially interpreted as a result of variations within the ice content of the permafrost, which can significantly influence the bulk rock thermal conductivity. To some extent the variability could also result from a remaining disturbance of the well temperatures from the drilling and construction of the wells within the permafrost interval.

[50] Despite the different scatter of values, the thermal conductivity profiles of the three Mallik wells show similar trends below the permafrost base (Figure 7). Analogous to the geothermal gradient profiles (section 3.3), the variations of thermal conductivity with depth show characteristic patterns, which are correlated with the lithological units described in section 2.

[51] The geothermal values of corresponding sections of the three Mallik 2002 wells are in close agreement (Table 4). Individual exceptions can be related to lithological variations between the wells. The average thermal conductivity values calculated from geothermal data range between 1.03 ± 0.15 W m^{-1} K^{-1} within the shale-rich lower part of unit 4 of Mallik 4L-38 and 2.88 ± 0.42 W m^{-1} K^{-1}

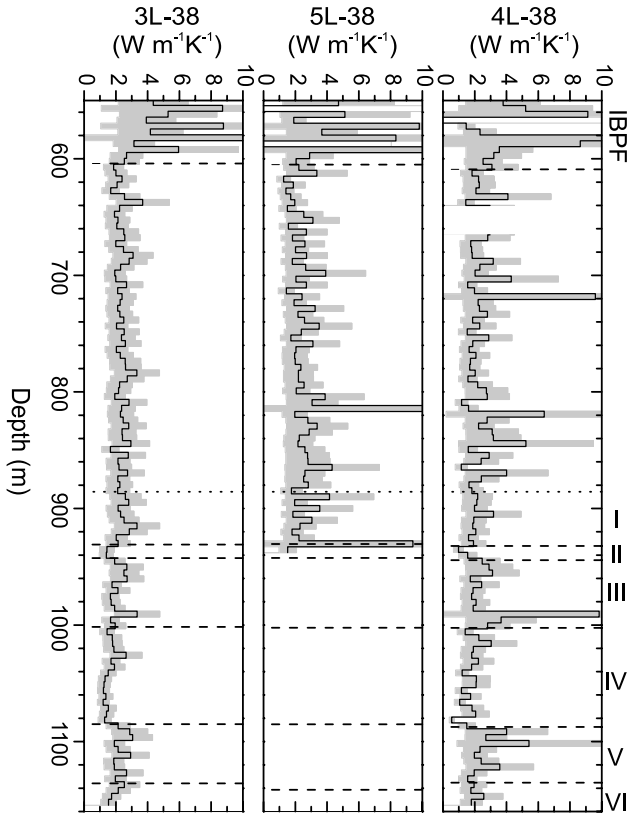

Figure 7. Thermal conductivity profiles calculated from the measured geothermal gradients (September 2003) and the local heat flow. Shaded areas indicate 95% confidence limits. Roman numerals indicate lithological units adopted from *Medioli et al.* [2005]. IBPF, base of ice-bearing permafrost.

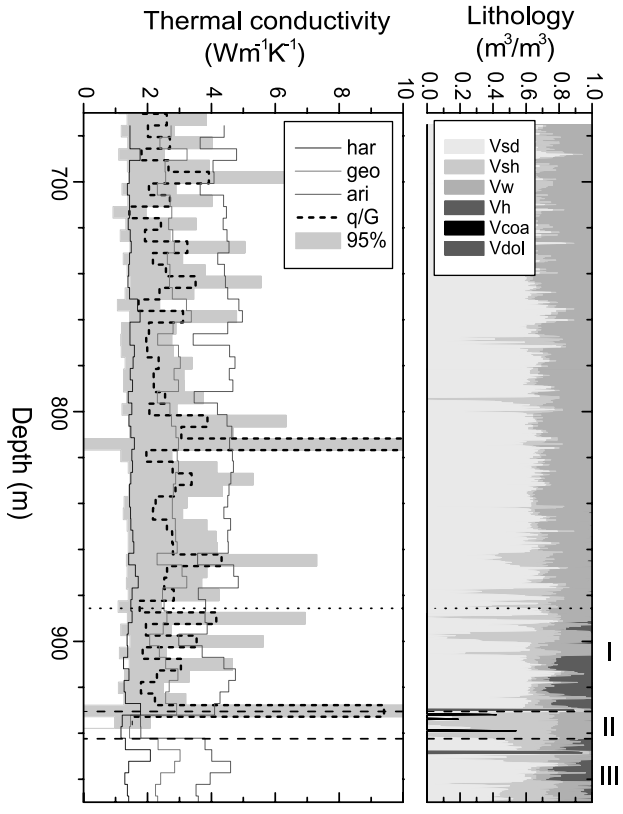

Figure 8. Comparison of thermal conductivity profiles calculated from mixing law models (arithmetic, geometric, and harmonic mean model) and 5-m average temperature gradients (Mallik 5L-38 well, September 2003), together with 95% confidence interval limits. For better comparability, the mixing law conductivities are correspondingly displayed as 5-m arithmetic average values. Roman numerals indicate lithological units adopted from *Medioli et al.* [2005]. See color version of this figure at back of this issue.

within the sand-rich and hydrate-bearing lower part of unit 1 of the Mallik 5L-38 well.

[52] Some prominent peaks of the calculated conductivities are clearly related to specific lithological features: The high conductivity interval at the base of unit 1 within the profile of the 5L-38 well correlates well with the occurrence of a dolomite-cemented sandstone interval (Figure 5). The low conductivity value near the base of unit 4 of the Mallik 4L-38 well corresponds to a 1.4 m thick coal layer at the adjacent Mallik 5L-38 well (Figure 5).

5.3. Comparison of Calculated Thermal Conductivity Profiles

[53] A comparison of the thermal conductivity profiles from the mixing law models and the geothermal data of the Mallik 5L-38 well is displayed in Figure 8. The data are only displayed for the depth interval between 670 and 970 m, in which both temperature and other logging data from the 5L-38 well were available.

[54] The average thermal conductivities calculated from the geothermal data almost exclusively lie within the bandwidth between the results of the arithmetic and harmonic mean models. This is interpreted as a good indicator that the assumptions about the local heat flow conditions, on which the calculation of thermal conductivities from geothermal data was based (section 5.2), are generally valid.

[55] The thermal conductivities calculated using the geometric mean model show a good agreement with the conductivities calculated from the geothermal gradient, both in terms of the magnitude of the absolute values as well as the amplitudes of variation. Except for a few isolated values, the geometric mean model values lie within the bandwidth of the 95% confidence limit of the conductivities calculated from the geothermal gradient. The results illustrate that reasonable estimates of thermal conductivity can be made using the geometric mean model, which previously has also been successfully applied for drill cuttings [*Sass et al.*, 1971] and isotropic sedimentary rocks [*Brigaud and Vasseur*, 1989]. *Troschke and Burkhardt* [1998] have observed a good agreement of measured and calculated thermal conductivities using the geometric mean model for sedimentary rocks with small differences of thermal conductivity between the rock matrix and the pore content. Within the suite of rocks under investigation at Mallik, the highest conductivity ratio of about 14 occurs between the sand fraction and the gas hydrate (Table 2), which is well below the limit of 20 stated by *Woodside and Messmer* [1961]. It should be noted that *Clauser and Huenges* [1995] have already reported a failure of the geometric mean model for conductivity contrasts above a ratio of 10.

[56] The good agreement of the geometric mean model values and the geothermal data also holds for the 23 m thick interval with high hydrate saturations of up to 87% at the base of unit 1 (Table 4). This is in accordance with the results of *Wright et al.* [2005], who performed measurements on rock samples and calculated effective thermal conductivity values using average lithological data of larger lithological units. They showed that reasonable thermal conductivity estimates of the hydrate-bearing sediments at Mallik were generated using the method proposed by *Johansen* [1975], which for saturated soils is equivalent to the geometric mean model applied in this work.

6. Conclusions

[57] The bulk rock thermal conductivity of the Mallik sediments can be quantitatively estimated by determining the lithological composition from logging data and applying mixing law models to calculate effective thermal conductivities. Results of the geometric mean model showed a good agreement with the thermal conductivity profiles derived from geothermal data, which were calculated from the measured geothermal gradients and an estimated local heat flow value of 55 mW m^{-2} based on Fourier's law of heat conduction. It is therefore concluded that the geometric mean model is generally applicable for the estimation of thermal conductivity of hydrate bearing sediments of the type encountered at Mallik, which are characterized by rather low thermal conductivity contrasts between the pore fillings and the rock matrix and by occurrences of disseminated methane hydrate with saturations of up to about 90%. Average thermal conductivity values of the sand intervals with high hydrate saturations range between 2.35 and 2.77 W m^{-1} K^{-1}.

[58] The results of the geometric mean model are in support of the apparently low influence of hydrate saturation on the bulk rock thermal conductivity deduced from the analysis of the geothermal gradients: The geometric mean model predicts a reduction of the bulk rock thermal conductivity of about 7% for a hydrate-saturated sand with 35% porosity compared to water saturated conditions. Variations within this order of magnitude could nevertheless not be determined from the available geothermal data because of the relatively large error, which to a large extent results from the uncertainty of the heat flow estimate. This rather large uncertainty also precludes a comparison of the results of more physically based thermal conductivity models, such as the modified version of the resistor model equation [*Woodside and Messmer*, 1961; *Huang and Fan*, 2005], or the method proposed by *Revil* [2000]. Within the low range of thermal conductivity contrasts under investigation, all of these models would show rather small differences in their results (i.e., below 20% compared to the results of the geometric mean model), which cannot be resolved on the basis of the current data set in hand. Therefore precision measurements of thermal conductivity on hydrate-bearing sediments under controlled laboratory conditions are recommended, including investigations of the influence of hydrate composition and microstructure, as well as the saturation within a porous medium on the bulk rock thermal conductivity. Nevertheless, on the basis of the improved knowledge about thermal conductivity, which is the main factor influencing the static temperature field, the road is now paved for studying the transient temperature response of hydrate-bearing sediments and heat transport processes during the formation and/or decomposition of gas hydrate.

[59] **Acknowledgments.** This is publication GEOTECH-191 of the R&D-Programme GEOTECHNOLOGIEN funded by the German Ministry of Education and Research (BMBF) and German Research Foundation (DFG), grant G0556A. The Mallik 2002 Gas Hydrate Production Research Well Program participants include seven partners (Geological Survey of Canada (GSC), Japan National Oil Corporation (JNOC), GeoForschungs-Zentrum Potsdam (GFZ), U.S. Geological Survey (USGS), U.S. Department of Energy (USDOE), India Ministry of Petroleum and Natural Gas (MOPNG), and BP-Chevron-Burlington joint venture group) and was supported by the International Continental Scientific Drilling Program (ICDP). J. Schrötter (GFZ Potsdam) assisted during the DTS installation at Mallik. F. M. Nixon, J. F. Wright (Geological Survey of Canada), and the staff at the Inuvik Research Centre provided invaluable logistical support during the October 2002 and September 2003 postfield site visits. B. Medioli kindly provided the data from the grain size and XRD analyses. The manuscript greatly benefited from the critical comments of the Associate Editor and two anonymous reviewers.

References

Beck, A. E. (1988), Methods for determining thermal conductivity and thermal diffusivity, in *Handbook of Terrestrial Heat-Flow Density Determination*, edited by R. Haenel, L. Rybach, and L. Stegena, pp. 87–124, Springer, New York.

Bily, C., and J. W. L. Dick (1974), Naturally occurring gas hydrates in the Mackenzie Delta, N.W.T, *Bull. Can. Pet. Geol.*, *22*(3), 340–352.

Brigaud, F., and G. Vasseur (1989), Mineralogy, porosity and fluid control on thermal conductivity of sedimentary rocks, *Geophys. J. Int.*, *98*(3), 525–542.

Clauser, C., and E. Huenges (1995), Thermal conductivity of rocks and minerals, in *Rock Physics and Phase Relations: A Handbook of Physical Constants*, *Ref. Shelf*, vol. 3, edited by T. J. Ahrens, pp. 105–126, AGU, Washington, D. C.

Collett, T. S. (2001), A review of well-log analysis techniques used to assess gas-hydrate-bearing reservoirs, in *Natural Gas Hydrates: Occurrence, Distribution, and Detection*, *Geophys. Monogr. Ser.*, vol. 124, edited by C. K. Paull and W. P. Dillon, pp. 189–210, AGU, Washington, D. C.

Collett, T. S., M. W. Lee, S. R. Dallimore, and W. F. Agena (1999), Seismic- and well-log-inferred gas hydrate accumulations on Richards Island, in *Scientific Results From JAPEX/JNOC/GSC Mallik 2L-38 Gas Hydrate Research Well, Mackenzie Delta, Northwest Territories, Canada*, edited by S. R. Dallimore, T. Uchida, and T. S. Collett, *Bull. Geol. Surv. Can.*, *544*, 357–376.

Cook, J. G., and M. J. Laubitz (1981), The thermal conductivity of two clathrate hydrates, paper presented at 17th International Thermal Conductivity Conference, Natl. Inst. of Stand. and Technol., Gaithersburg, Md.

Dallimore, S. R., and T. S. Collett (1999), Regional gas hydrate occurrences, permafrost conditions, and Cenozoic geology, Mackenzie Delta area, in *Scientific Results From JAPEX/JNOC/GSC Mallik 2L-38 Gas Hydrate Research Well, Mackenzie Delta, Northwest Territories, Canada*, edited by S. R. Dallimore, T. Uchida, and T. S. Collett, *Bull. Geol. Surv. Can.*, *544*, 31–43.

Dallimore, S. R., and T. S. Collett (Eds.) (2005), Scientific Results From the Mallik 2002 Gas Hydrate Production Research Well Program, Mackenzie Delta, Northwest Territories, Canada, *Bull. Geol. Surv. Can.*, *585*.

Dallimore, S. R., T. S. Collett, and T. Uchida (1999), Overview of science program, JAPEX/JNOC/GSC Mallik 2L-38 gas hydrate research well, in *Scientific Results From JAPEX/JNOC/GSC Mallik 2L-38 Gas Hydrate Research Well, Mackenzie Delta, Northwest Territories, Canada*, edited by S. R. Dallimore, T. Uchida, and T. S. Collett, *Bull. Geol. Surv. Can.*, *544*, 11–17.

Dallimore, S. R., T. S. Collett, M. Weber, and T. Uchida (2002), Drilling program investigates permafrost gas hydrates, *Eos Trans. AGU*, *83*(18), 193, 198.

Farouki, O. T. (1981), Thermal properties of soils, *Tech. Rep. CRREL Monogr. 81-1*, U.S. Army Corps of Eng., Cold Reg. Res. and Eng. Lab., Hanover, N. H.

Förster, A., J. Schrötter, D. F. Merriam, and D. D. Blackwell (1997), Application of optical-fiber temperature logging: An example in a sedimentary environment, *Geophysics*, *62*(4), 1107–1113.

Hancock, S., T. S. Collett, S. R. Dallimore, T. Satoh, T. Inoue, E. Huenges, J. Henninges, and B. Weatherill (2005), Overview of thermal-stimulation production-test results for the JAPEX/JNOC/GSC et al. Mallik 5L-38 gas hydrate production research well, in *Scientific Results From the Mallik 2002 Gas Hydrate Production Research Well Program, Mackenzie Delta, Northwest Territories, Canada*[CD-ROM], edited by S. R. Dallimore and T. S. Collett, *Bull. Geol. Surv. Can.*, *585*.

Hartog, A., and G. Gamble (1991), Photonic distributed sensing, *Phys. World*, *3*, 45–49.

Henninges, J., J. Schrötter, K. Erbas, and E. Huenges (2005), Temperature field of the Mallik gas hydrate occurrence: Implications on phase changes and thermal properties, in *Scientific Results From the Mallik 2002 Gas Hydrate Production Research Well Program, Mackenzie Delta, Northwest Territories, Canada*[CD-ROM], edited by S. R. Dallimore and T. S. Collett, *Bull. Geol. Surv. Can.*, *585*.

Huang, D., and S. Fan (2005), Measuring and modeling thermal conductivity of gas hydrate-bearing sand, *J. Geophys. Res.*, *110*, B01311, doi:10.1029/2004JB003314.

Hurtig, E., J. Schrötter, S. Grosswig, K. Kühn, B. Harjes, W. Wieferig, and R. P. Orrell (1993), Borehole temperature measurements using distributed fibre optic sensing, *Sci. Drill.*, *3*(6), 283–286.

Johansen, O. (1975), Thermal conductivity of soils, Ph.D. thesis, Univ. of Trondheim, Trondheim, Norway.

Kleinberg, R. L., C. Flaum, C. Straley, P. G. Brewer, G. E. Malby, E. T. Peltzer III, G. Friederich, and J. P. Yesinowski (2003), Seafloor nuclear magnetic resonance assay of methane hydrate in sediment and rock, *J. Geophys. Res.*, *108*(B3), 2137, doi:10.1029/2001JB000919.

Kleinberg, R. L., C. Flaum, and T. S. Collett (2005), Magnetic resonance log of JAPEX/JNOC/GSC et al. Mallik 5L-38 gas hydrate production research well: Gas hydrate saturation, growth habit, and relative permeability, in *Scientific Results From the Mallik 2002 Gas Hydrate Production Research Well Program, Mackenzie Delta, Northwest Territories, Canada*[CD-ROM], edited by S. R. Dallimore and T. S. Collett, *Geol. Surv. Can. Bull.*, *585*.

Kulenkampff, J., and E. Spangenberg (2005), Physical properties of cores from the JAPEX/JNOC/GSC et al. Mallik 5L-38 gas hydrate production research well under simulated in situ conditions using the Field Laboratory Experimental Core Analysis System (FLECAS), in *Scientific Results From the Mallik 2002 Gas Hydrate Production Research Well Program, Mackenzie Delta, Northwest Territories, Canada*[CD-ROM], edited by S. R. Dallimore and T. S. Collett, *Geol. Surv. Can. Bull.*, *585*.

Majorowicz, J. A., and S. L. Smith (1999), Review of ground temperatures in the Mallik field area: A constraint to the methane hydrate stability, in *Scientific Results From JAPEX/JNOC/GSC Mallik 2L-38 Gas Hydrate*

Research Well, Mackenzie Delta, Northwest Territories, Canada, edited by S. R. Dallimore, T. Uchida, and T. S. Collett, *Geol. Surv. Can. Bull.*, *544*, 45–56.

Medioli, B. E., N. Wilson, S. R. Dallimore, D. Paré, P. Brennan-Alpert, and H. Oda (2005), Sedimentology of the cored interval, JAPEX/JNOC/GSC et al. Mallik 5L-38 gas hydrate production well, Mackenzie Delta, Northwest Territories, in *Scientific Results From the Mallik 2002 Gas Hydrate Production Research Well Program, Mackenzie Delta, Northwest Territories, Canada*[CD-ROM], edited by S. R. Dallimore and T. S. Collett, *Geol. Surv. Can. Bull.*, *585*.

Revil, A. (2000), Thermal conductivity of unconsolidated sediments with geophysical applications, *J. Geophys. Res.*, *105*, 16,749–16,768.

Rider, M. H. (1996), *The Geological Interpretation of Well Logs*, 2nd ed., Whittles Publ., Caithness, Scotland.

Ruppel, C. (2000), Thermal state of the gas hydrate reservoir, in *Natural Gas Hydrate in Oceanic and Permafrost Environments*, edited by M. D. Max, pp. 29–42, Springer, New York.

Sass, J. H., A. H. Lachenbruch, and R. J. Munroe (1971), Thermal conductivity of rocks from measurements on fragments and its application to heat-flow determinations, *J. Geophys. Res.*, *76*, 3391–3401.

Sloan, E. D. (1998), *Clathrate hydrates of natural gases*, 2nd ed., 705 pp., CRC Press, Boca Raton, Fla.

Somerton, W. H. (1992), *Thermal Properties and Temperature-Related Behavior of Rock/Fluid Systems*, *Dev. Pet. Sci.*, vol. 37, 257 pp., Elsevier, New York.

Stoll, R. D., and G. M. Bryan (1979), Physical properties of sediments containing gas hydrates, *J. Geophys. Res.*, *84*, 1629–1634.

Troschke, B., and H. Burkhardt (1998), Thermal conductivity models for two-phase systems, *Phys. Chem. Earth*, *23*(3), 351–355.

Waite, W. F., B. J. deMartin, S. H. Kirby, J. Pinkston, and C. D. Ruppel (2002), Thermal conductivity measurements in porous mixtures of methane hydrate and quartz sand, *Geophys. Res. Lett.*, *29*(24), 2229, doi:10.1029/2002GL015988.

Woodside, W., and J. H. Messmer (1961), Thermal conductivity of porous media, *J. Appl. Phys.*, *32*, 1688–1699.

Wright, J. F., F. M. Nixon, S. R. Dallimore, J. Henninges, and M. M. Côté (2005), Thermal conductivity of sediments within the gas-hydrate-bearing interval at the JAPEX/JNOC/GSC et al. Mallik 5L-38 gas hydrate production research well, in *Scientific Results From the Mallik 2002 Gas Hydrate Production Research Well Program, Mackenzie Delta, Northwest Territories, Canada*[CD-ROM], edited by S. R. Dallimore and T. S. Collett, *Bull. Geol. Surv. Can.*, *585*.

H. Burkhardt, Technische Universität Berlin, Fachgebiet Angewandte Geophysik, Sekr. ACK 2, Ackerstraße 71-76, D-13355 Berlin, Germany.

J. Henninges and E. Huenges, GeoForschungsZentrum Potsdam, Telegrafenberg, D-14473 Potsdam, Germany. (janhen@gfz-potsdam.de)

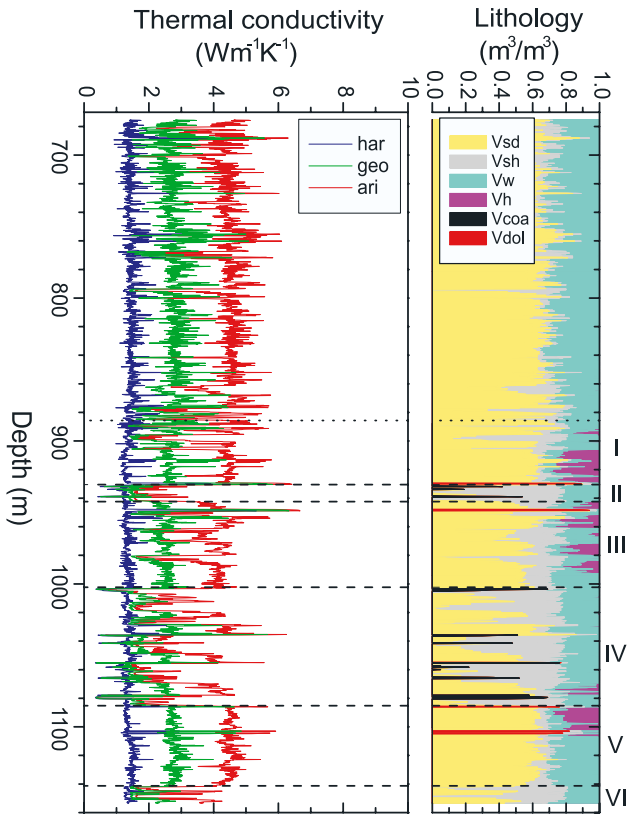

Figure 6. Comparison of thermal conductivity profiles for Mallik 5L-38 well calculated from arithmetic, geometric, and harmonic mean mixing law models. Lithological composition is derived from logging data. Roman numerals indicate lithological units adopted from *Medioli et al.* [2005].

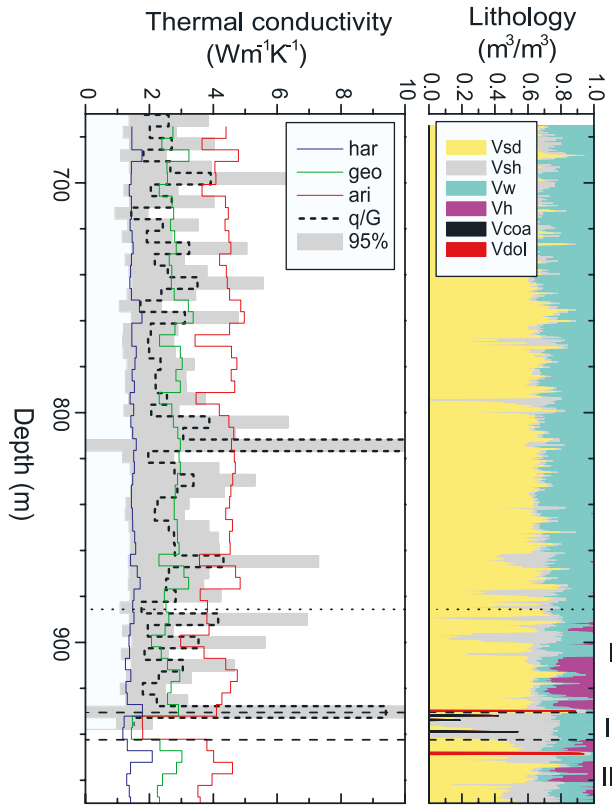

Figure 8. Comparison of thermal conductivity profiles calculated from mixing law models (arithmetic, geometric, and harmonic mean model) and 5-m average temperature gradients (Mallik 5L-38 well, September 2003), together with 95% confidence interval limits. For better comparability, the mixing law conductivities are correspondingly displayed as 5-m arithmetic average values. Roman numerals indicate lithological units adopted from *Medioli et al.* [2005].